

**SENSITIVE VLBI CONTINUUM AND H I ABSORPTION  
OBSERVATIONS OF NGC 7674:  
FIRST SCIENTIFIC OBSERVATIONS WITH THE COMBINED  
ARRAY VLBA, VLA and ARECIBO**

Emmanuel Momjian<sup>1,2</sup>

`momjian@pa.uky.edu`

Jonathan D. Romney<sup>1</sup>

`jromney@nrao.edu`

Christopher L. Carilli<sup>1</sup>

`ccarilli@nrao.edu`

and

Thomas H. Troland<sup>2</sup>

`troland@pa.uky.edu`

**ABSTRACT**

We present phase-referenced VLBI observations of the radio continuum emission from, and the neutral hydrogen 21 cm absorption toward, the Luminous Infrared Galaxy NGC 7674. The observations were carried out at 1380 MHz using the Very Long Baseline Array, the phased Very Large Array, and the 305-m Arecibo radio telescope. These observations constitute the first scientific use of the Arecibo telescope in a VLBI observation with the VLBA. The high- and low-resolution radio continuum images reveal several new continuum structures in the nuclear region of this galaxy. At  $\sim$ 100 mas resolution, we distinguish six continuum structures extending over 1.4 arcsec (742 pc), with a total flux density of 138 mJy. Only three of these structures were known previously. All these structures seem to be related to AGN activity. The overall S-shaped pattern that

---

<sup>1</sup>National Radio Astronomy Observatory, P O Box O, Socorro, NM 87801.

<sup>2</sup>University of Kentucky, Department of Physics and Astronomy, Lexington, KY 40506.

the radio structures seem to form could be the result of the interstellar medium diverting the outcoming jets from the central AGN. However, we cannot rule out the possibility of a black hole merger that could result in a similar structural pattern. At the full resolution of the array ( $11 \times 5$  mas), we only detect two of the six continuum structures. Both are composed of several compact components with brightness temperatures on the order of  $10^7$  K. While it is possible that one of these compact structures could host an AGN, they could also be shock-like features formed by the interaction of the jet with compact interstellar clouds in the nuclear region of this galaxy. Complex H I absorption is detected with our VLBI array at both high and low angular resolution. Assuming that the widest H I feature is associated with a rotating H I disk or torus feeding a central AGN, we estimate an enclosed dynamical mass of  $\sim 7 \times 10^7 M_\odot$ , comparable to the value derived from the hidden broad H $\beta$  emission in this galaxy. The narrower H I lines could represent clumpy neutral hydrogen structures in the H I torus. The detection of H I absorption toward some of the continuum components, and its absence toward others, suggest an inclined H I disk or torus in the central region of NGC 7674. The overall averaged H I spectrum toward the continuum structures with H I absorption is very consistent with the Arecibo single dish H I absorption spectrum at 3.3' resolution.

*Subject headings:* galaxies: individual (NGC 7674) — galaxies: jets — galaxies: Seyfert — radio continuum: galaxies — radio lines: galaxies — galaxies: nuclei

## 1. INTRODUCTION

At bolometric luminosities above  $10^{11} L_\odot$ , infrared galaxies become the most numerous objects in the local universe ( $z \leq 0.3$ ). These galaxies further subdivide into luminous (LIRGs<sup>3</sup>), ultraluminous (ULIRGs<sup>4</sup>), and hyperluminous (HyLIRGs<sup>5</sup>) infrared galaxies (Sanders & Mirabel 1996). A large fraction of these IR galaxies are interacting or merger systems, and this fraction seems to increase with luminosity (Sanders et al. 1988). The bulk of the energy radiated by these sources is infrared emission from warm dust grains heated by a central power source or sources. The critical question concerning these galaxies is whether

---

<sup>3</sup>LIRG:  $10^{11} L_\odot \leq L_{\text{IR}}(8 - 1000 \mu\text{m}) < 10^{12} L_\odot$

<sup>4</sup>ULIRG:  $10^{12} L_\odot \leq L_{\text{IR}}(8 - 1000 \mu\text{m}) < 10^{13} L_\odot$

<sup>5</sup>HyLIRG:  $L_{\text{IR}}(8 - 1000 \mu\text{m}) \geq 10^{13} L_\odot$

the dust is heated by a nuclear starburst, or an active galactic nucleus (AGN), or a combination of both. Mid-infrared spectroscopic studies on a sample of ULIRGs by Genzel et al. (1998), suggest that 70%–80% of these galaxies are predominantly powered by recently formed massive stars, and 20%–30% by a central AGN. These authors conclude further that at least half of these ULIRGs are probably powered by both an AGN and a starburst in a 1–2 kpc diameter circumnuclear disk or ring.

In this paper, we present VLBI continuum and H I absorption observations on the type-2 Seyfert galaxy NGC 7674 (Mrk 533, Arp 182, UGC 12608). This galaxy is a nearby LIRG with an infrared luminosity of  $L_{\text{IR}} = 3.1 \times 10^{11} L_{\odot}$  (González Delgado, Heckman, & Leitherer 2001). Optical observations of NGC 7674 show a nearly face-on spiral with an inclination angle of  $i = 31^\circ$  (Verdes-Montenegro et al. 1997). This galaxy is classified as Sbc pec (de Vaucouleurs, de Vaucouleurs, & Corwin 1976). It is the brightest member of the well isolated Hickson 96 compact galaxy group (Hickson 1982), which consists of four interacting galaxies with a mean heliocentric velocity of  $8760 \text{ km s}^{-1}$  and a low velocity dispersion ( $\sigma_v = 160 \text{ km s}^{-1}$ ) (Verdes-Montenegro et al. 1997). The two largest members in this group, NGC 7674 (H96a) and NGC 7675 (H96b), are separated by a projected distance of 2.2 arcmin. The observed features in NGC 7674, as revealed in optical images, can be accounted for by tidal interactions with its companion galaxies in the group (Verdes-Montenegro et al. 1997).

The Very Large Array 15 GHz observations of NGC 7674 by Unger et al. (1988) showed a triple radio source with components defined as eastern, central, and western, but their 1666 MHz EVN+MERLIN observations at 20 mas resolution only revealed the central and the western components. These authors identified the central component as the radio nucleus and the western component as a radio lobe moving outward through the interstellar medium. However, their 20 mas VLBI image did not reveal any clear jet structure connecting the central and the western components, which are separated by  $\sim 0.5 \text{ arcsec}$ . MERLIN observations by Beswick, Pedlar, & McDonald (2002) at  $0.^{\prime\prime}27 \times 0.^{\prime\prime}15$  and 1.4 GHz also revealed a triple radio source consistent with the 15 GHz VLA observations (Unger et al. 1988).

Single dish Arecibo observations by Mirabel (1982) at 3.3 arcmin resolution showed two clearly separated H I absorption features that are blueshifted with respect to a wider emission line. The absorption lines have full velocity widths at 20% of  $63$  and  $45 \text{ km s}^{-1}$ , while the emission line has  $344 \text{ km s}^{-1}$ . The two H I absorption features are at  $\sim 8600 \text{ km s}^{-1}$  and  $\sim 8546 \text{ km s}^{-1}$ , respectively. However, the neutral hydrogen interferometric observations with MERLIN at  $0.^{\prime\prime}27 \times 0.^{\prime\prime}15$  and  $32 \text{ km s}^{-1}$  (Beswick, Pedlar, & McDonald 2002) revealed a single H I absorption feature against the central component with an optical depth of 0.21 and a velocity width of  $114 \text{ km s}^{-1}$  at half maximum, centered at  $8623 \text{ km s}^{-1}$ . No H I absorption was reported toward the eastern or the western components in these MERLIN

observations.

We adopt a distance of 115.6 Mpc to NGC 7674, assuming  $H_0 = 75 \text{ km s}^{-1} \text{ Mpc}^{-1}$ . At this distance 1 mas corresponds to 0.53 pc.

## 2. OBSERVATIONS AND DATA REDUCTION

The observations were carried out at 1380 MHz on September 15, 2001 using NRAO's<sup>6</sup> Very long Baseline Array (VLBA) and the phased Very Large Array (VLA), and NAIC's 305-m Arecibo radio telescope<sup>7</sup>. These observations constitute the first scientific use of the Arecibo radio telescope with the VLBA after the installation and the successful testing of the VLBA4 recording system. Two adjacent 8 MHz baseband channel pairs were used in these observations, both with right and left-hand circular polarizations, sampled at two bits. The first baseband channel pair was centered close to the frequency of the neutral hydrogen 21 cm line, which is at a heliocentric redshift of  $z = 0.0287$ , or  $cz = 8600 \text{ km s}^{-1}$ . The velocity coverage of each baseband channel was  $\sim 1738 \text{ km s}^{-1}$ . The data were correlated at the VLBA correlator in Socorro, NM with 512-point spectral resolution per baseband channel, and 5.1 seconds correlator integration time. The total observing time was 12 hours, with the 305-m Arecibo radio telescope participating for 140 minutes. Table 1 summarizes the parameters of these observations.

The inclusion of both the phased VLA (Y27) and Arecibo were essential in these observations in two respects. One is the overall image sensitivity (the rms thermal noise level), and the other is the short to moderate-length sensitive baselines necessary to image large scale structures. While including the phased VLA in the VLBA improves the image sensitivity by a factor of  $\sim 2.4$ , the sensitivity improves by a factor of  $\sim 7.1$  when both the phased VLA and Arecibo are added to the VLBA. This latter sensitivity improvement is achieved only during the time when Arecibo is observing. In our observations, where Arecibo participated for about 20% of the total observing time, the image sensitivity was  $\sim 4.2$  times better than the VLBA alone for the whole observing time. Also, the 305-m Arecibo radio telescope provided the 3rd sensitive short baseline in our observations, this baseline is Arecibo–Saint Croix with 238 km length. The other two sensitive short baselines are the Y27–Pie Town (52 km) and Y27–Los Alamos (226 km). Short sensitive baselines are critical to image extended

---

<sup>6</sup>The National Radio Astronomy Observatory is a facility of the National Science Foundation operated under cooperative agreement by Associated Universities, Inc.

<sup>7</sup>The Arecibo Observatory is part of the National Astronomy and Ionosphere Center, which is operated by Cornell University under a cooperative agreement with the National Science Foundation.

continuum structures as well as the H I absorption toward these structures.

Data reduction and analysis were performed using the Astronomical Image Processing System (AIPS) and the Astronomical Information Processing System (AIPS++).

Along with the target source NGC 7674, the compact source J2329+0834 was observed as a phase reference with a cycle time of 150 seconds, 100 seconds on the target source and 50 seconds on the phase calibrator. The source J2334+0736 was used for amplitude calibration, and 3C 454.3 (J2253+1608) was observed as a fringe finder and used to determine the initial fringe delays and to calibrate the bandpass.

After applying *a priori* flagging and manually excising integrations affected by interference, ionospheric corrections were applied using the AIPS task “TECOR”. Amplitude calibration was performed using measurements of the antenna gain and the system temperature of each station. The delay solutions for 3C 454.3 were applied and a bandpass calibration was performed. To image the continuum of the target source, its line-free channels were averaged to a single spectral channel with a total width of 14 MHz. The phase calibrator J2329+0834 was self-calibrated in both amplitude and phase and imaged in an iterative cycle. The self-calibration solutions of J2329+0834 were applied on the continuum data of the target source NGC 7674. Due to the high rms noise values obtained after applying the self-calibration solutions of the phase reference source to NGC 7674, we performed self calibration on the continuum data set of the target source itself. This resulted in a significant improvement in the signal-to-noise ratio. The self calibration solutions of both the phase calibrator and the target source were later applied to the line data, in which every two channels were averaged to increase the sensitivity. The resulting channel separation of the H I data cube was 31.25 kHz (6.986 km s<sup>-1</sup>). The continuum emission was subtracted from the spectral-line visibility data using the AIPS task “UVLSF”. The spectral-line data were then analyzed at various spatial and spectral resolutions. Deconvolution of the images in the continuum and line data sets was performed using the Clark “CLEAN” algorithm as implemented in the AIPS task “IMAGR”. Optical-depth  $\tau(\nu)$  cubes were calculated from the H I absorption image cubes and continuum images with a similar resolution as  $\tau(\nu) = -\ln[1 - I_{\text{line}}(\nu)/I_{\text{continuum}}]$ .

Along with these observations, we also reduced and analyzed archival VLA data of NGC 7674 from 1986. These A-array observations with program ID AH 233 were carried out at 15 GHz.

### 3. RESULTS AND ANALYSIS

#### 3.1. *The Radio Continuum*

Figure 1 shows moderate and high resolution continuum images of the nuclear region in NGC 7674 at 1380 MHz. The top image has a resolution of 20 mas (10.6 pc) obtained with natural grid weighting (ROBUST = 5 in AIPS task “IMAGR”). The resolution of this image is comparable to the VLBI image of Unger et al. (1988). We distinguish six structures in this image, only three of them previously known. We identify these three structures, following Unger et al. (1988), as western (W), central (C) and eastern (E) components. In our image, C is the brightest, E is the diffuse emission region just to the east of C, and W is the second brightest peak. In addition to these components, we detect a clear collimated jet structure (J) connecting the C and W components, and two diffuse emission regions, one located to the north-east of E that we designate the northeastern component (NE), and another to the south-west of W, the southwestern component (SW). The linear extent of the whole nuclear region in the plane of the sky is  $\sim 1.4$  arcsec (742 pc), and the total flux is  $\sim 138$  mJy. We also reduced the VLA data from these 1.38 GHz observations, which were performed in the DnC configuration and yielded a resolution of  $40''.5 \times 17''.3$  (PA  $80^\circ$ ). The total flux density of the source at this resolution is  $\sim 230$  mJy. Our analysis of the 15 GHz archival VLA data resulted in a marginal detection ( $3\sigma$ ) of the newly discovered components NE and SW.

The bottom images in Figure 1 are of C (*left*) and W (*right*) at the full resolution of our array, which is  $11 \times 5$  mas ( $5.8 \times 2.7$  pc). These two images were obtained with grid weighting ROBUST =  $-1$ . The other components identified in our 20 mas image are resolved.

Figures 2 shows the continuum structure in gray scale with half-maximum ellipses for gaussians fitted to the structures seen in C (*left*) and W (*right*). These gaussian components provide a convenient measure of source structure even if they do not necessarily represent discrete physical structures. Parameters of the gaussian fits are listed in Tables 2 and 3, for components C and W, respectively. Column 1 in both these tables lists the gaussians seen in Figure 2, and column 2 their positions relative to the brightest peak in each image. Columns 3 and 4 show the peak and the total flux densities of the fitted gaussian functions, respectively. Columns 5, 6, and 7 list the half-power ellipse axes and the position angles. Column 8 shows the derived brightness temperatures of these components. All Gaussian fitting parameters were obtained using the tool “IMAGEFITTER” in AIPS++.

An image of the nuclear region of NGC 7674 at lower resolution (Figure 3) clearly shows the diffuse components seen at 20 mas (Figure 1-top). The restoring beam in Figure 3 is  $92 \times 76$  mas ( $48.8 \times 40.3$  pc). Table 4 summarizes the characteristics of the continuum structures labeled in Figure 3. The positions (col. [2]) are relative to the central component

(C). Columns 3 and 4 show the peak and the total flux densities of the fitted gaussian functions, respectively. Columns 5, 6, and 7 list the half-power ellipse axes and the position angles. No good gaussian fit was obtainable for the jet structure; thus we have estimated its flux density and its size from the residual image left after subtracting the gaussian fittings of the other components. The reported size of the jet component is its linear extent on the plane of the sky.

The accuracy of the phase calibrator position is important in phase-referencing observations (Walker 1999), which allow the determination of the absolute position of the target source and its components, if any, from the position of the calibrator. The positions reported in all the above mentioned images and tables are obtained from the position of the phase-reference source J2329+0834. The position of J2329+0834 is from the VLBA calibrator survey (Beasley et al. 2002), with positional accuracy of  $\sim 0.7$  mas in right ascension and  $\sim 1.3$  mas in declination.

Table 5 summarizes the magnetic field and pressure values of the radio continuum components seen in NGC 7674 at low angular resolution using the minimum energy condition (Miley 1980). These properties were derived using the 1380 MHz total flux densities of these components (Table 4) and their angular extents on the plane of the sky, and assuming a path length through the source on the line of sight equal to the major axis of the component. Spectral indices of the C, E, and W components were obtained from Beswick, Pedlar, & McDonald (2002). For the NE and SW components, we derived spectral indices from the marginal detection of these structures at 15 GHz with the VLA and our 1380 MHz VLBI results convolved to the beam size of the 15 GHz observations. Spectral indices of all five components are steep ( $> 0.6$ ;  $S \propto \nu^{-\alpha}$ ). No spectral index estimate was possible for the jet (J) structure, hence it was excluded from these calculations.

### 3.2. The H I Absorption

All images reported in this section are reconstructed with natural grid weighting in the AIPS task “IMAGR”. The H I data cube was imaged using Hanning smoothing to improve the signal-to-noise ratio. Thus, although the channel separation is about  $7 \text{ km s}^{-1}$ , the effective velocity resolution is  $\sim 14 \text{ km s}^{-1}$ . The H I results are described separately for high and low spatial resolutions, because of the distinctive characteristics of the absorption at these two scales.

### 3.2.1. H I Absorption at High Spatial Resolution

Figure 4 shows the naturally weighted high resolution continuum images of the central (*top*) and the western (*bottom*) components in NGC 7674 with averaged H I absorption spectra against several background continuum regions in both C and W. The angular resolution is  $17 \times 5$  mas ( $9 \times 2.7$  pc). The rms noise in the continuum images is  $\sim 30 \mu\text{Jy beam}^{-1}$ . While the spectra obtained toward W show no H I absorption, all the spectra obtained against the components in C show significant absorption. The rms noise in the H I image cube is  $\sigma \simeq 260 \mu\text{Jy beam}^{-1}$ .

Figure 5 shows optical depth  $\tau(\nu)$  images in the velocity range  $8626.7$ – $8529.0 \text{ km s}^{-1}$ . These images explicitly show the variation of the H I opacity against the central component of NGC 7674 at high spatial resolution. The images are obtained by blanking areas where the flux density of the continuum image is below  $2.5 \text{ mJy beam}^{-1}$  (i.e. less than 15% of the peak flux), or the H I absorption is below  $1.04 \text{ mJy beam}^{-1}$  (i.e.  $4 \sigma$ ).

We distinguish four main absorption features in both the spectra H I and the optical depth images. They are identified in Figure 4. Their velocity widths range between  $18$  and  $98 \text{ km s}^{-1}$  at half maximum, with optical depths between  $0.164$  and  $0.412$ . Table 6 summarizes the physical characteristics of these four H I absorption features, obtained by fitting gaussian functions to the optical depth spectra averaged over regions where the absorption features are seen. The fits were performed using the tool “IMAGEPROFILEFITTER” in AIPS++. The velocities (col. [2]) refer to the center velocities of these features. The widths of these lines (col. [3]) are the full widths at half peak optical depth. Column 4 is the peak optical depth value of each feature.  $N_{\text{HI}}/T_s$  of each peak (col. [5]) is calculated as  $N_{\text{HI}}/T_s (\text{cm}^{-2} \text{ K}^{-1}) = 1.823 \times 10^{18} \int \tau(v) dv$ , with  $\int \tau(v) dv = 1.06 \tau_{\text{peak}} \Delta v_{\text{FWHM}}$  for gaussian profiles. The column densities  $N_{\text{HI}}$  (col. [6]) are derived assuming a spin temperature  $T_s$  of  $100 \text{ K}$ .

The first two H I absorption components listed in Table 6 are mainly seen against the continuum component C1. The weaker of these two is wider,  $98.3 \text{ km s}^{-1}$ . The other two features are narrower, and are seen against the continuum component C3. Only the strongest H I absorption feature, the first component in Table 7, has a measurable velocity gradient as shown in the velocity field image with continuum contours superimposed (Figure 6-*top*). Figure 6-*bottom* shows a position velocity (P-V) diagram along a cut in position angle  $14^\circ$ . This diagram suggests a velocity gradient of  $\sim 30.3 \text{ km s}^{-1}$  along  $\sim 18.4 \text{ pc}$  (i.e.  $\sim 1647 \text{ km s}^{-1} \text{ kpc}^{-1}$ ).

Figures 7*a*-7*b* are  $N_{\text{HI}}/T_s$  images in the velocity range  $8626.7$ – $8529.0 \text{ km s}^{-1}$ . Figure 7*a* is a color-scale image and contours of  $N_{\text{HI}}/T_s$ . Figure 7*b* shows the same  $N_{\text{HI}}/T_s$  color-scale

image with continuum contours superimposed for positional reference.

### 3.2.2. H I Absorption at Low Spatial Resolution

Figure 8 shows the naturally weighted low resolution continuum image of the nuclear region in NGC 7674 at 1380 MHz and  $129 \times 108$  mas ( $68.4 \times 57.2$  pc) resolution. Averaged H I absorption spectra are shown against the previously identified continuum components. The rms noise level of the continuum and the H I data are 85 and  $570 \mu\text{Jy beam}^{-1}$ , respectively. We notice clear H I absorption detections (greater than  $3\sigma=1.68 \text{ mJy beam}^{-1}$ ) toward C, E, and NE. We do not detect any absorption against SW, W, or J. The strongest H I feature is centered at  $8600.3 \pm 1.1$ . This value is consistent with the strongest feature seen in the Arecibo single dish spectrum at  $3.3$  resolution (Mirabel 1982); however, it is lower by  $23 \text{ km s}^{-1}$  from the value reported by Beswick, Pedlar, & McDonald (2002) at  $0.27 \times 0.15$  resolution with MERLIN. The non-detection of H I absorption in the MERLIN observations toward E (Beswick, Pedlar, & McDonald 2002) could be simply a result of their low velocity resolution, which is  $32 \text{ km s}^{-1}$ , compared to  $14 \text{ km s}^{-1}$  achieved in our sensitive VLBI observations.

Figure 9 shows optical depth  $\tau(\nu)$  images in the velocity range  $8619.6$ – $8522.0 \text{ km s}^{-1}$ . These images explicitly show the variation of the H I opacity against C, E, and NE at low spatial resolution. The images are obtained by blanking areas where the flux density of the continuum image is below  $6 \text{ mJy beam}^{-1}$  (i.e. less than 12% of the peak flux), or the H I absorption is below  $2.28 \text{ mJy beam}^{-1}$  (i.e.  $4\sigma$ ).

Figures 10a-10b are  $N_{\text{HI}}/T_s$  images in the velocity range  $8626.7$ – $8522.0 \text{ km s}^{-1}$ . Figure 10a is a color-scale image and contours of  $N_{\text{HI}}/T_s$ . Figure 10b shows the same  $N_{\text{HI}}/T_s$  color-scale image with continuum contours superimposed for positional reference.

The top panel of Figure 11 is the velocity field of the H I absorption at low spatial resolution superimposed on the continuum contours, and the bottom panel is the averaged H I absorption spectrum over the region where absorption signals are detected.

From the H I absorption images and spectra at low resolution (Figures 8, 9, 10, & 11-*top*), we distinguish four main absorption features. They are identified in Figure 8. Their velocity widths range between  $23$  and  $165 \text{ km s}^{-1}$  at half maximum, with optical depths between  $0.1$  and  $0.65$ . Table 7 summarizes the physical characteristics of these four H I absorption features, obtained by fitting gaussian functions to the optical depth spectra averaged over regions where the absorption features are seen. The fittings were performed using the tool “IMAGEPROFILEFITTER” in AIPS++. The velocities (col. [2]) refer to peaks of these

features. The widths of these lines (col. [3]) are the full widths at half peak optical depth. Column 4 is the peak optical depth value of each feature as seen in the averaged spectra.  $N_{\text{HI}}/T_s$  of each peak (col. [5]) is calculated as  $N_{\text{HI}}/T_s$  ( $\text{cm}^{-2} \text{ K}^{-1}$ ) =  $1.823 \times 10^{18} \int \tau(v)dv$ , with  $\int \tau(v)dv = 1.06\tau_{\text{peak}}\Delta v_{\text{FWHM}}$  for gaussian profiles. The column densities  $N_{\text{HI}}$  (col. [6]) are derived assuming  $T_s = 100 \text{ K}$ .

At this low resolution, the absorption feature with the highest velocity is seen toward C. The velocity of the H I line seen against E is lower than the velocities of the H I features seen against C and NE.

The bottom panel of Figure 11 is the integrated H I absorption profile against the whole region where H I signals are detected at  $129 \times 108$  mas resolution. While the high velocity feature is mainly due to the H I absorption toward C, the lower velocity feature arises from the H I absorption toward both E and NE. The double peak pattern seen in our spectrum is very consistent with the observed H I absorption profile with Arecibo at  $3'3$  resolution (Mirabel 1982) in both velocity and width values. It should be noted that the MERLIN observations of Beswick, Pedlar, & McDonald (2002) did not detect the lower velocity component seen in this spectrum.

## 4. DISCUSSION

### 4.1. *The Radio Continuum*

At moderate resolution (tens of mas), the nuclear region of NGC 7674 is composed of several continuum structures extending over 0.75 kpc (Figure 1-*top*, & Figure 3). At high resolution, the continuum results (Figure 1-*bottom*, & Figure 2) show several compact continuum structures in both the central (C) and the western (W) components, with brightness temperatures  $\geq 10^7 \text{ K}$ . The total flux density of all the radio components seen in our VLBI array is  $\sim 138 \text{ mJy}$  and represents only 60% of the total flux density seen at lower resolution with the VLA, and 72% of the total flux density detected with MERLIN (Beswick, Pedlar, & McDonald 2002). These differences suggest the existence of diffuse emission not detected by our VLBI array, which may be extensions to the continuum structures seen in our observations. In the next two sections, we will discuss the possible nature of all the continuum structures seen in this galaxy.

#### 4.1.1. Is there a starburst in NGC 7674?

Most characteristics of the continuum structures in NGC 7674, both at large and small scales, seem to be related to AGN activity and not to a nuclear or circumnuclear starburst. Calculations by Yun, Reddy, & Condon (2001) clearly indicate that this galaxy does not obey the radio-FIR correlation well known for “normal” galaxies, where the main energy source is not due to a supermassive black hole (Condon 1992). This correlation is represented by the quantity  $q$  as defined by Helou, Soifer, & Rowan-Robinson (1985):

$$q = \log \{ [FIR / (3.75 \times 10^{12})] / S_{1.4 \text{ GHz}} \}, \quad (1)$$

where  $FIR$  is given by:

$$FIR = 1.26 \times 10^{-14} (2.58 S_{60 \text{ } \mu\text{m}} + S_{100 \text{ } \mu\text{m}}). \quad (2)$$

For “normal galaxies”,  $q = 2.34 \pm 0.01$  (Yun, Reddy, & Condon 2001). Furthermore, these authors conclude that a value of  $q \leq 1.64$  indicates the presence of an AGN. For NGC 7674, they report  $q = 1.53$ .

Nonetheless, evidence does exist for star formation. The optical spectroscopic studies of González Delgado, Heckman, & Leitherer (2001) indicate the presence of young/intermediate-age (a few Myr to a few 100 Myr) stars in the nuclear region of NGC 7674, and the question we seek to answer at this stage is whether any of the emission structures we observe in the nuclear region of NGC 7674 could be related to starburst activity. For this purpose, we compare the expected star formation rates from  $H\alpha$  and IR emissions with the nonthermal radio continuum emission. The star formation rates will be calculated using a Salpeter IMF which has the form  $\psi(M) \propto M^{-2.35}$  (Salpeter 1955) with mass limits 0.1 and  $100 M_\odot$  as given by Kennicutt (1998), taking into account that the nonthermal radio emission would result from Type II supernova explosions that require stars with masses  $\geq 8 M_\odot$ .

The optical spectroscopic observations of de Grijp et al. (1992) suggest that the  $H\alpha$  luminosity of the nuclear region of NGC 7674 is  $5.3 \times 10^{34}$  W. Assuming all the  $H\alpha$  emission is due to starburst activity and using the relationship between the star formation rate (SFR) and the  $H\alpha$  luminosity (Kennicutt 1998), which has the form:

$$SFR (M_\odot \text{ yr}^{-1}) = 7.9 \times 10^{-35} L_{H\alpha} (\text{W}), \quad (3)$$

we derive an SFR of  $4.2 M_\odot \text{ yr}^{-1}$ .

To calculate the SFR from the IR emission, we assume all the IR luminosity is only due to starburst, and use the relationship given by Kennicutt (1998):

$$SFR (M_\odot \text{ yr}^{-1}) = 4.5 \times 10^{-44} L_{\text{IR}} (\text{erg s}^{-1}). \quad (4)$$

The IR luminosity of NGC 7674 is  $3.1 \times 10^{11} L_\odot$  (González Delgado, Heckman, & Leitherer 2001), and the resulting SFR is  $54 M_\odot \text{ yr}^{-1}$ .

The SFR calculations based on radio luminosity will take into account the flux densities of the three diffuse radio components, namely E, NE and SW. The radio luminosity of these three components is  $8.6 \times 10^{22} \text{ W Hz}^{-1}$ , and it is all due to nonthermal radiation because of the mere fact that they are detected by our VLBI array. VLBI arrays, even with the extremes of sensitivity we were able to achieve in these observations, currently lack the sensitivity to detect thermal emission. To derive the SFR from the radio luminosity, we first calculate the supernova rate using the empirical relation of Condon & Yin (1990) that relates the observed Galactic non-thermal luminosity ( $L_{\text{NT}}$ ) to the supernova rate  $\nu_{\text{SN}}$ :

$$\left( \frac{L_{\text{NT}}}{10^{22} \text{ W Hz}^{-1}} \right) = 13 \left( \frac{\nu}{\text{GHz}} \right)^{-0.8} \left( \frac{\nu_{\text{SN}}}{\text{yr}^{-1}} \right). \quad (5)$$

We derive  $\nu_{\text{SN}} = 0.86 \text{ yr}^{-1}$ . The SFR can be calculated from the supernova rate by using and combining the following expressions:

$$\nu_{\text{SN}} = \int_{m_{\text{sn}}}^{100M_\odot} \psi(m) \, dm, \quad (6)$$

with  $m_{\text{sn}} = 8 M_\odot$  for Type II supernovae, and

$$SFR = \int_{0.1M_\odot}^{100M_\odot} m \psi(m) \, dm. \quad (7)$$

These two equations result in an SFR of  $\sim 116 M_\odot \text{ yr}^{-1}$ .

The very low SFR obtained from the H $\alpha$  emission could result from extinction. However, the SFR estimated from the luminosity of the three diffuse radio components in NGC 7674 is still greater than the SFR calculated from the whole IR luminosity of the nuclear region. Thus, we conclude that these continuum components are more likely related to AGN activity, with no strong indication for a nuclear or circumnuclear starburst in our VLBI results.

#### 4.1.2. The reason for the S-shaped pattern in NGC 7674, and the location of the AGN

Our continuum results at  $\sim 100$  mas resolution (Figure 3) revealed the previously unknown continuum structures NE and SW. The overall shape of the continuum components in the nuclear region seem to form an S-shaped pattern. A detailed study on galaxies with similarly shaped radio structures was reported by Merritt & Ekers (2002). The authors point out that the orientation of a black hole's spin axis could dramatically change even in a minor

merger, leading to a flip in the direction of any associated jet. Thus, following their discussion, it is possible that the components NE and SW are jet structures that formed before a possible black hole merger in NGC 7674. However, it is also possible that the interstellar medium could be diverting the outcoming jets from the AGN and causing them to form the NE and SW structures and the overall S-shaped pattern we are seeing in NGC 7674.

The black hole merger scenario would imply that the AGN may be located in the central component (C). However, the few high angular resolution observations available on this source are not enough to identify the AGN component in this galaxy. Early 18 cm VLBI observations at 20 mas resolution (Unger et al. 1988) tentatively identified the component C to host the AGN, because of its brightness and proximity to the optical center of the galaxy. At a few mas resolution, the VLBA observations at 2.3 & 8.4 GHz (J. F. Gallimore & C. Murray-Kreuzan 2002, private communication) detected two of the three compact continuum features seen in the component C at 21 cm. These components seem to match the C1 and C3 structures seen in our 21 cm observations. The measured total fluxes at 2.3 & 8.4 GHz were noisy, and the derived spectral indices for the two components were neither flat, nor steep. For  $S \propto \nu^{-\alpha}$ , these values were  $\alpha(C1) = 0.53$  and  $\alpha(C3) = 0.35$ . Thus, it is not clear whether either of these two components is hosting the AGN. Also, no information is available on the third structure seen in the central component. While it is possible that any of these compact sources could be hosting the AGN, they could also be shock-like features formed because of the interaction between the jet and compact interstellar clouds in the nuclear region of NGC7674.

#### 4.2. The H I Absorption

Our observations reveal the details of the H I absorption against the radio continuum emission in NGC 7674 both at high angular resolution ( $17 \times 5$  mas, Figures 4 to 7), and low resolution ( $129 \times 108$  mas, Figures 8 to 11). The H I absorption at high angular resolution is composed of several features. The strongest H I line is the only feature with a measurable velocity gradient (Figure 6-top panel). The P-V diagram in position angle  $14^\circ$  (Figure 6-bottom panel), shows a velocity gradient of  $1647 \text{ km sec}^{-1} \text{ kpc}^{-1}$ . If this measured gradient is arising from H I gas in a rotating disk or torus, then at a radius of 17.4 mas (9.2 pc), assuming a Keplerian motion, the enclosed dynamical mass would be  $5 \times 10^5 M_\odot$ . However, calculation based on the observed width of the hidden broad H $\beta$  emission line suggests a black hole mass in the range  $(4.4 - 13.2) \times 10^7 M_\odot$ , assuming an optical depth for electron scattering between  $\tau_{\text{es}} = 0.1$  and 1 (Nishiura & Taniguchi 1998). This difference could be explained by a rotating H I disk, with only a small section of it being illuminated by the

background radio source. A similar explanation was put forward by Beswick, Pedlar, & McDonald (2002). These authors further suggested that the rotating H I disk should be edge-on, because of the non-detection of H I absorption toward the western or the eastern components seen on MERLIN scale.

However, our results clearly show H I absorption against E and NE, and no absorption against J, W, or SW (Figure 8). While a possible origin for the H I absorption toward E and NE could be neutral gas in intervening clouds far from the nuclear region of NGC 7674, the almost face-on orientation of the galaxy and the velocities of the detected H I features suggest that these H I absorption lines also arise within an H I disk or torus. Thus, this rotating H I disk around the central black hole should be inclined, i. e. should not be an edge-on structure.

Following the H I torus model illustrated by Peck (1999) which suggests the existence of dense neutral hydrogen clumps in the circumnuclear H I torus associated with a central AGN, it is very likely that the absorption features seen at both low and high angular resolution with velocity widths  $< 50 \text{ km s}^{-1}$  arise from such clumpy structures. Thus, the velocity gradient seen in Figure 6 for the H I feature with a width of  $35.4 \text{ km s}^{-1}$  at half maximum, could be due to turbulent motion or infall of a dense clumpy structure within the H I torus, and not represent the rotational motion around the black hole. The absorption seen toward E and NE components could also arise in such H I clumps within the torus. An indication for the clumpy H I torus can be seen from the optical depths and the velocity widths of the various H I components listed in Tables 6 and 7. The narrower H I features (i.e. 1, 3, 4, I, II, & IV), which also have higher optical depths ( $\gtrsim 0.3$ ), seem to represent the neutral hydrogen clumps in the torus, and the wider H I components (i.e. 2 & III), which have lower optical depths, seem to represent the rotating H I torus itself. Using virial considerations, the enclosed dynamical mass estimated from the widest H I feature ( $\Delta v_{\text{FWHM}} = 165 \text{ km s}^{-1}$ ) at a radius of about 10 pc is  $\sim 7 \times 10^7 M_{\odot}$ . This value is consistent with the dynamical mass derived from the hidden broad H $\beta$  emission by Nishiura & Taniguchi (1998).

#### 4.2.1. *The Location of the AGN: a more comprehensive picture*

Observations of NGC 7674 with the BeppoSAX X-ray observatory by Malaguti et al. (1998) resulted in an absorption column density of  $N_{\text{H}} \simeq 6 \times 10^{22} \text{ cm}^{-2}$ , which is derived from the hard X-ray spectrum. Comparing this column density with the values listed in column 5 of Tables 5 & 6 would suggest a spin temperature ( $T_{\text{s}}$ ) of at least 1000 K. Such a high value could be expected for the H I spin temperature if the absorption is actually tracing a warmer atomic medium in the AGN environment (Gallimore et al. 1999), where

the spin temperature can rise to several 1000 K before the hydrogen atoms are significantly ionized (Maloney, Hollenbach, & Tielens 1996).

However, the neutral hydrogen absorption studies in Seyfert galaxies by Gallimore et al. (1999) showed that the H I absorption in these galaxies generally avoids the nucleus, and it is more commonly seen against other radio components. This suggests that the absorption in the X-ray could be tracing different foreground gas than the absorption at 21 cm, and explains the higher column density in X-ray compared to the 21 cm H I absorption. This also suggests that the continuum structures associated with the H I absorption, namely C, E, and NE, are jet structures. This possibility is further supported by the steep spectra of these continuum structures seen at low resolutions discussed by Beswick, Pedlar, & McDonald (2002) and in section 3.1 of this work.

Based on the preceding discussion, we speculate that the AGN is located to the west of all the continuum structures that have H I absorption associated with them. This picture would exclude the W and SW components as AGN hosts, because of their steep spectra. Hence, a possible location for the AGN is in the J structure revealed for the first time in these sensitive VLBI observations. This implies that the two strongest sources, C and W, are possibly radio lobes or hot spots, with the AGN located somewhere in between these two structures, but simply free-free absorbed at 1.38 GHz.

### 4.3. The age of the AGN in NGC 7674

Using the above model for the location of the AGN and the nature of the C and W components, we can estimate the age of the AGN in NGC 7674. For this purpose, we follow the discussion in Carilli & Barthel (1996) for non-relativistic high Mach jets. The standard assumption is that the bulk of the kinetic energy supplied by the jet is  $L_j = L_R/\epsilon$ , where  $L_R$  is the total radio lobe luminosity, and  $\epsilon$  is an efficiency factor for converting bulk kinetic energy into radio luminosity. The value of  $\epsilon$  is  $\leq 0.4$ , but it is more likely to be considerably less (Carilli & Barthel (1996) and references therein). Also, the jet must do work ( $W \approx P_L \times V_L$ ) to expand the ambient medium, where  $P_L$  is the lobe pressure derived using the minimum energy argument and  $V_L$  is the volume of the lobe. For the central component in NGC 7674,  $L_R = 8.5 \times 10^{40} \text{ erg s}^{-1}$ ,  $P_L = 12.3 \times 10^{-9} \text{ dyn cm}^{-2}$ , and  $V_L = 6.84 \times 10^{61} \text{ cm}^3$ . The source lifetime  $t_s$ , which could be indicative of the AGN lifetime, would be  $t_s \approx W/L_j \simeq 0.3/\epsilon \text{ Myr}$ . Thus, the estimated age of the AGN in NGC 7674 is few Myr, which is approximately the age of the young stellar population reported by Genzel et al. (1998).

## 5. CONCLUSIONS

We have presented the results of phase-referenced VLBI observations, using the VLBA, the phased VLA, and the 305-m Arecibo radio telescope, of the 21 cm continuum emission and the H I absorption in the central  $\sim 0.75$  kpc of the type-2 Seyfert galaxy NGC 7674, which is also classified as a LIRG. The inclusion of both the phased VLA and Arecibo was a key factor in the success of these observations.

The low resolution continuum images reveal previously unknown structures in the nuclear region of this galaxy. The total VLBI flux density at 1380 MHz is 138 mJy, and represents only 60% of the total flux seen with the VLA at a lower resolutions, suggesting the existence of diffuse emission not detected by our VLBI array. All the observed structures seem to be related to AGN activity with no strong indication of a nuclear or circumnuclear starburst. The overall S-shaped pattern that the radio structures seem to form could be the result of the interstellar medium diverting the outcoming jets from the central AGN. However, we cannot rule out the possibility of a black hole merger that could result in a similar structural pattern.

The high resolution images show at least seven compact sources in the components defined in the literature as central (C) and western (W). Their brightness temperature is  $\gtrsim 10^7$  K. These compact sources are probably shock-like features formed due to the interaction of the jet with interstellar gas. However, one of these compact sources may actually be hosting the AGN. The currently available studies are insufficient to confirm such a possibility. Future sensitive multi-frequency VLBI observations will be the most direct way to identify a possible AGN component in the nuclear region of NGC 7674.

Both low and high resolution VLBI images show a complex H I absorption with several peaks. The detected H I lines have column densities on the order of  $10^{21}$  cm $^{-2}$ , assuming a spin temperature of 100 K. At low resolution, we distinguish at least four H I absorption peaks detected against the central (C), the eastern (W), and the northeastern (NE) components. No H I absorption was seen against the jet (J), the western (W), or the southwestern (SW) component. All these absorption features seem to arise in the H I disk or torus associated with the AGN. While the narrow features ( $\Delta v_{\text{FWHM}} < 50$  km s $^{-1}$ ) could represent clumpy neutral hydrogen structures in the H I torus, the widest absorption feature ( $\Delta v_{\text{FWHM}} = 165$  km s $^{-1}$ ) may represent the rotating torus itself. If the widest H I feature (component III) is rotationally broadened by a massive central object, the implied mass is about  $10^7$  M $_{\odot}$ . This value of the derived enclosed mass is very consistent with the black hole mass calculated from the width of the hidden broad H $\beta$  emission line. The detection of H I absorption toward some of the continuum components, and its absence toward others, suggest that the H I disk or torus is inclined and not edge-on as previously had been suggested.

## 6. ACKNOWLEDGMENTS

The authors thank C. Salter and T. Ghosh for their contributions to the success of the Arecibo part of these VLBI observations and their helpful suggestions for processing the Arecibo data. This research has made use of the NASA/IPAC Extragalactic Database (NED) which is operated by the Jet Propulsion Laboratory, California Institute of Technology, under contract with the National Aeronautics and Space Administration. E. M. is grateful for support from NRAO through the Pre-doctoral Research Program. T. H. T. and E. M. acknowledge NSF support through grant AST 99-88341.

## REFERENCES

Beasley, A. J., Gordon, D., Peck, A. B., Petrov, L., MacMillan, D. S., Fomalont, E. B., & Ma, C. 2002 *ApJS*, 141, 13

Beswick, R. J., Pedlar, A., McDonald, A. R. 2002, *MNRAS*, 335, 1091

Carilli, C. L., & Barthel, P. D. 1996, *A&A Rev.*, 7, 1

Condon, J. J., & Yin, Q. F. 1990, *ApJ*, 357, 97.

Condon, J. J. 1992, *ARA&A*, 30, 575

de Grijp, M. H. K., Keel, W. C., Miley, G. K., Goudfrooij, P., Lub, J. 1992, *A&AS*, 96, 389

de Vaucouleurs, G., de Vaucouleurs, A., & Corwin, J. R. 1976, Second Reference Catalogue of Bright Galaxies, University of Texas, Austin

Gallimore, J. F., Baum, S. A., O'Dea, C. P., Pedlar, A., & Brinks, E. 1999, *ApJ*, 524, 684

Genzel, R., et al. 1998, *ApJ*, 498, 579

González Delgado, R. M., Heckman, T., & Leitherer, C. 2001, *ApJ*, 546, 865

Helou, G., Soifer, B. T., & Rowan-Robinson, M. 1985, *ApJ*, 298, L7

Hickson, P. 1982, *ApJ*, 255, 382

Kennicutt, R. C. 1998, *ARA&A*, 36, 189

Malaguti, G. et al. 1998, *A&A*, 331, 519

Maloney, P. R., Hollenbach, D. J., Tielens, A. G. G. M. 1996, *ApJ*, 466, 561

Merritt, D., & Ekers, R. D., 2002, *Science*, 297, 1310

Miley, G. 1980, *ARA&A*, 18, 165.

Mirabel, I. F. 1982, *ApJ*, 260, 75

Nishiura, S., Taniguchi, Y. 1998, *ApJ*, 499, 134

Peck, A. B. 1999, Ph. D. thesis, NMIMT

Salpeter, E. E. 1955, *ApJ*, 121, 161

Sanders, D. B., Soifer, B. T., Elias, J. H., Madore, B. F., Matthews, K., Neugebauer, G., & Scoville, N. Z. 1988, *ApJ*, 325, 74

Sanders, D. B., & Mirabel, I. F. 1996, *ARA&A*, 34, 749

Unger et al. 1988, *MNRAS*, 234, 754

Verdes-Montenegro, L., del Olmo, A., Perea, J., Athanassoula, E., Márquez, I., & Augarde, R. 1997, *A&A*, 321, 409

Walker, C. R. 1999, in *Synthesis Imaging in Radio Astronomy II*, ed. G. B. Taylor, C. L. Carilli, & R. A. Perley (San Francisco: ASP), 433

Yun, Min S., Reddy, N. A., & Condon, J. J. 2001, *ApJ*, 554, 803

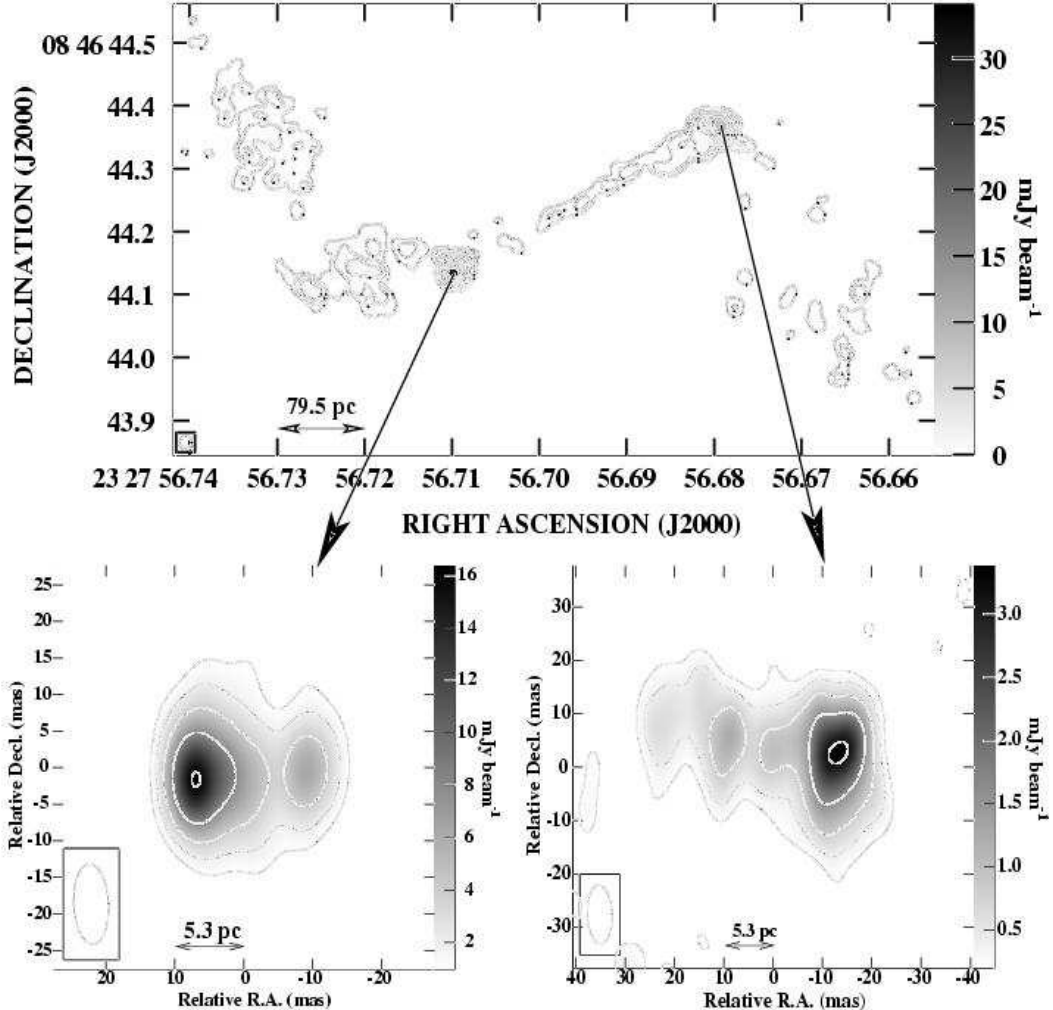


Fig. 1.— *Top:* Continuum image of the nuclear region in NGC 7674 at 1380 MHz. A Gaussian taper falling to 30% at  $8\text{ M}\lambda$  in the U direction and  $15\text{ M}\lambda$  in the V direction was applied. The restoring beam size is 20 mas. The peak flux is  $34\text{ mJy beam}^{-1}$ , and the contour levels are at  $-5, 5, 10, 20, 40, \dots, 640$  times the rms noise level, which is  $34\text{ }\mu\text{Jy beam}^{-1}$ . *Bottom:* Full resolution continuum images of the central (*left*) and the western (*right*) components in NGC 7674. The restoring beam size is  $11 \times 5$  mas in position angle  $3^\circ$ . The peak fluxes are indicated with the wedge on the right side of each image. The rms noise in both images is  $67\text{ }\mu\text{Jy beam}^{-1}$ . The contour levels of the bottom-left image are at  $-1, 1, 2, 4, 8, 16\text{ mJy beam}^{-1}$ , and the  $(0,0)$  point is  $\alpha(\text{J2000}) = 23^{\text{h}}27^{\text{m}}56^{\text{s}}7097$ ,  $\delta(\text{J2000}) = 08^{\circ}46'44\overset{''}{.}135$ . The contour levels of the bottom-right image are at  $-0.2, 0.2, 0.4, 0.8, 1.6, 3.2\text{ mJy beam}^{-1}$ , and the  $(0,0)$  point is  $\alpha(\text{J2000}) = 23^{\text{h}}27^{\text{m}}56^{\text{s}}6798$ ,  $\delta(\text{J2000}) = 08^{\circ}46'44\overset{''}{.}367$ .

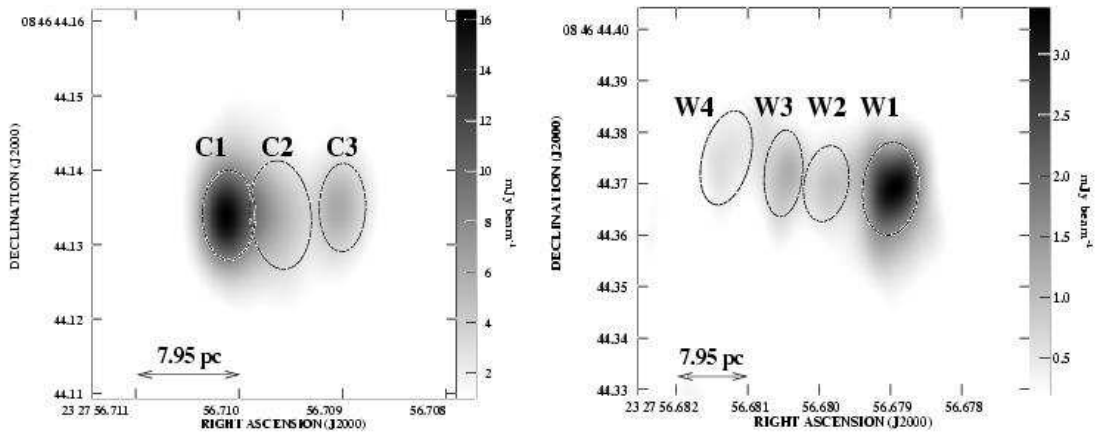


Fig. 2.— Gray scale continuum image of the central (*left*) and western (*right*) components in NGC 7674 at  $11 \times 5$  mas resolution. The ellipses represent the half-power gaussians fitted to these components.

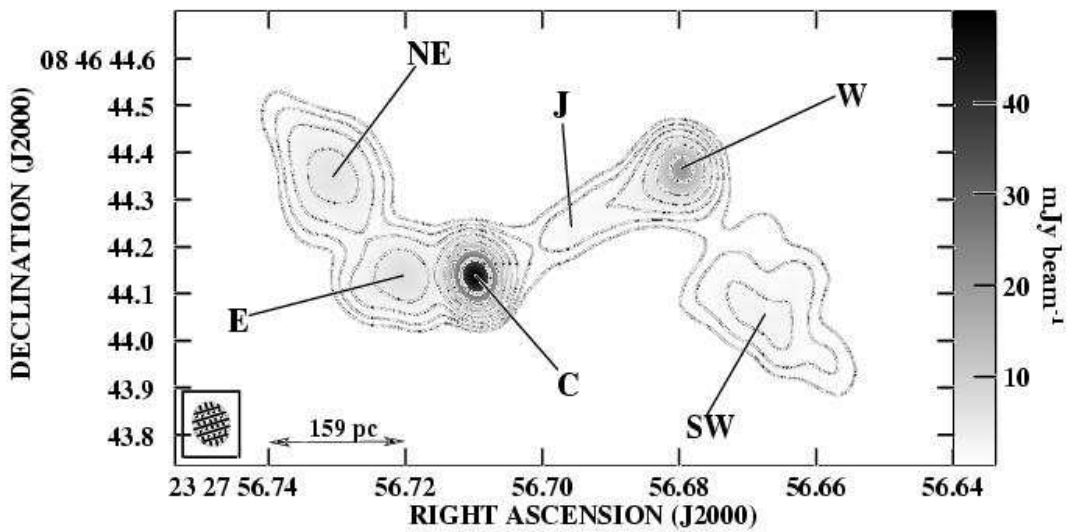


Fig. 3.— Continuum image of the nuclear region in NGC 7674 at 1380 MHz. The restoring beam size is  $92 \times 76$  mas in position angle  $16.5^\circ$ . A two dimensional Gaussian taper falling to 30% at  $2.5 \text{ M}\lambda$  was applied. The contour levels are  $-0.5, 0.5, 1, 2, 4, 8, 16, 32 \text{ mJy beam}^{-1}$ . The rms noise level is  $78 \mu\text{Jy beam}^{-1}$ . The properties of the labeled components are listed in Table 4.

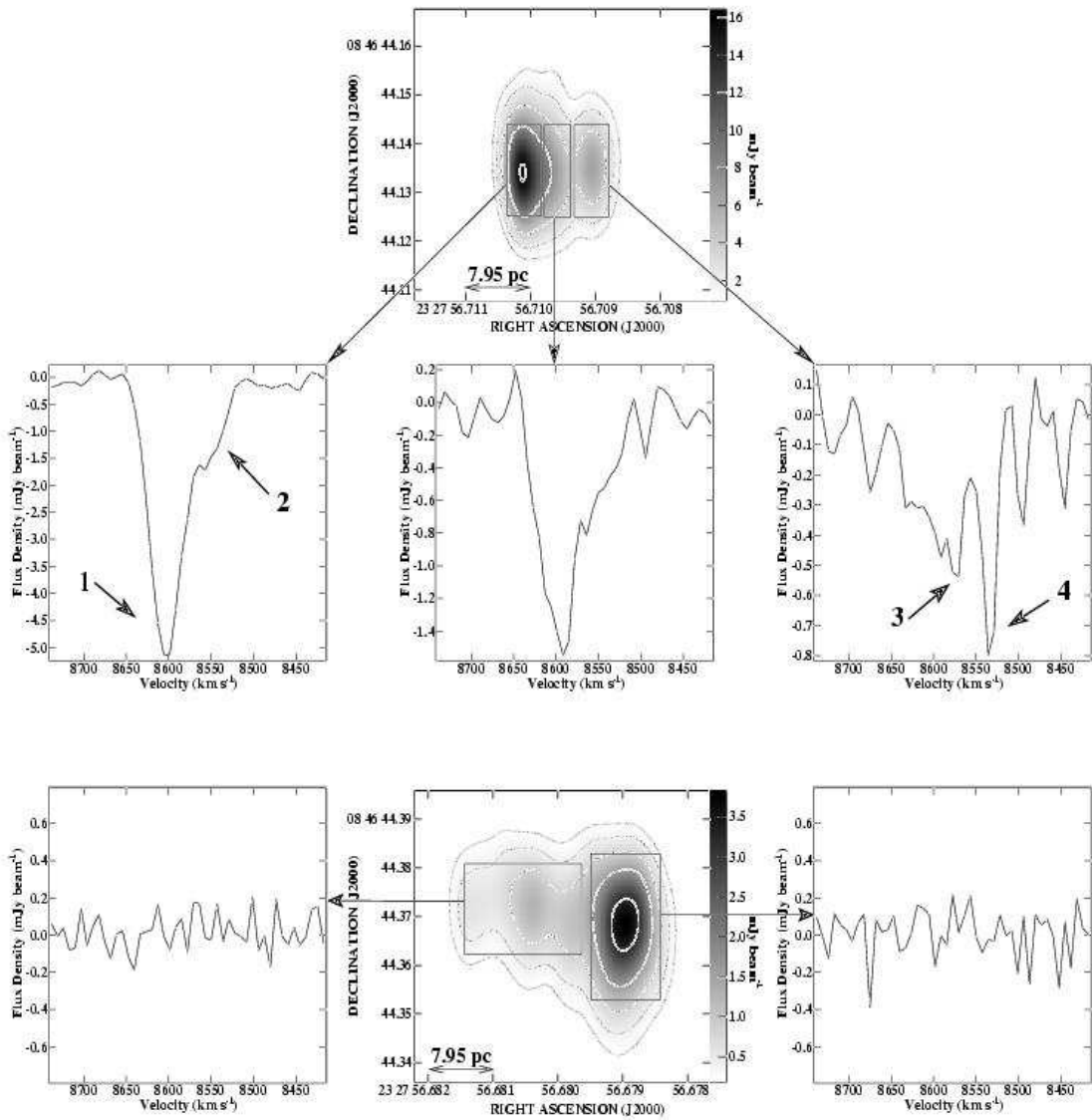


Fig. 4.— H I absorption spectra obtained at various locations against the central (*top*) and the western (*bottom*) components of NGC 7674 at 1380 MHz. The effective velocity resolution of the H I spectra is  $14 \text{ km s}^{-1}$ . The restoring beam size of both the continuum and the H I is  $17 \times 5 \text{ mas}$  in position angle  $3^\circ$ . The contour levels of the continuum images are the same as in Figure 1-*bottom*.

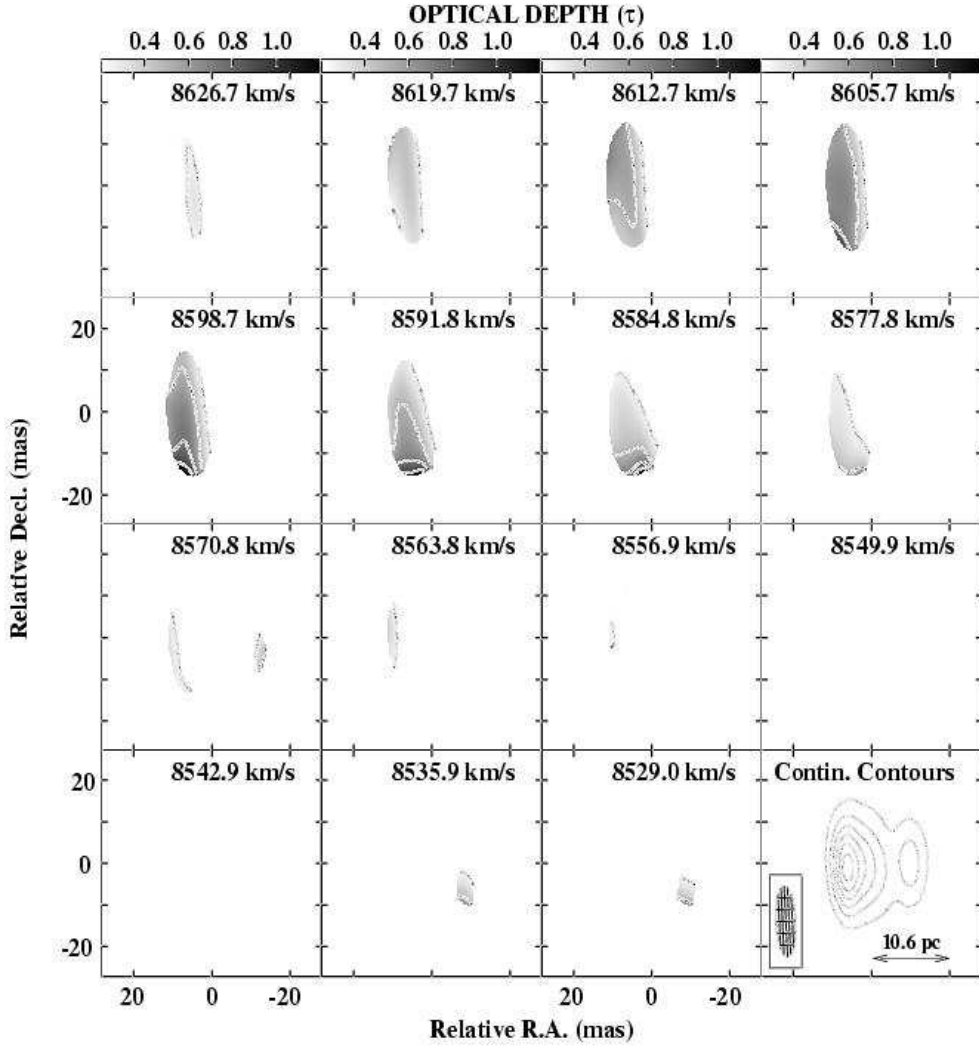


Fig. 5.— High resolution gray-scale and contour H I optical depth channel images toward the central component in NGC 7674 in the velocity range  $8626.7$ – $8529.0$  km s $^{-1}$ . The gray-scale range is indicated by the step wedge at the top of the images; the contour levels are 0.25, 0.5, 0.75, and 1.0. At the bottom-right corner a contour image of the continuum is shown as a positional reference with levels at 2.5, 5, 7.5, 10, 12.5 and 15 mJy beam $^{-1}$ . The restoring beam in these images is  $17 \times 5$  in position angle  $3^\circ$ . The point (0,0) is  $\alpha(\text{J2000}) = 23^{\text{h}}27^{\text{m}}56^{\text{s}}.7097$ ,  $\delta(\text{J2000}) = 08^\circ 46' 44''.135$ .

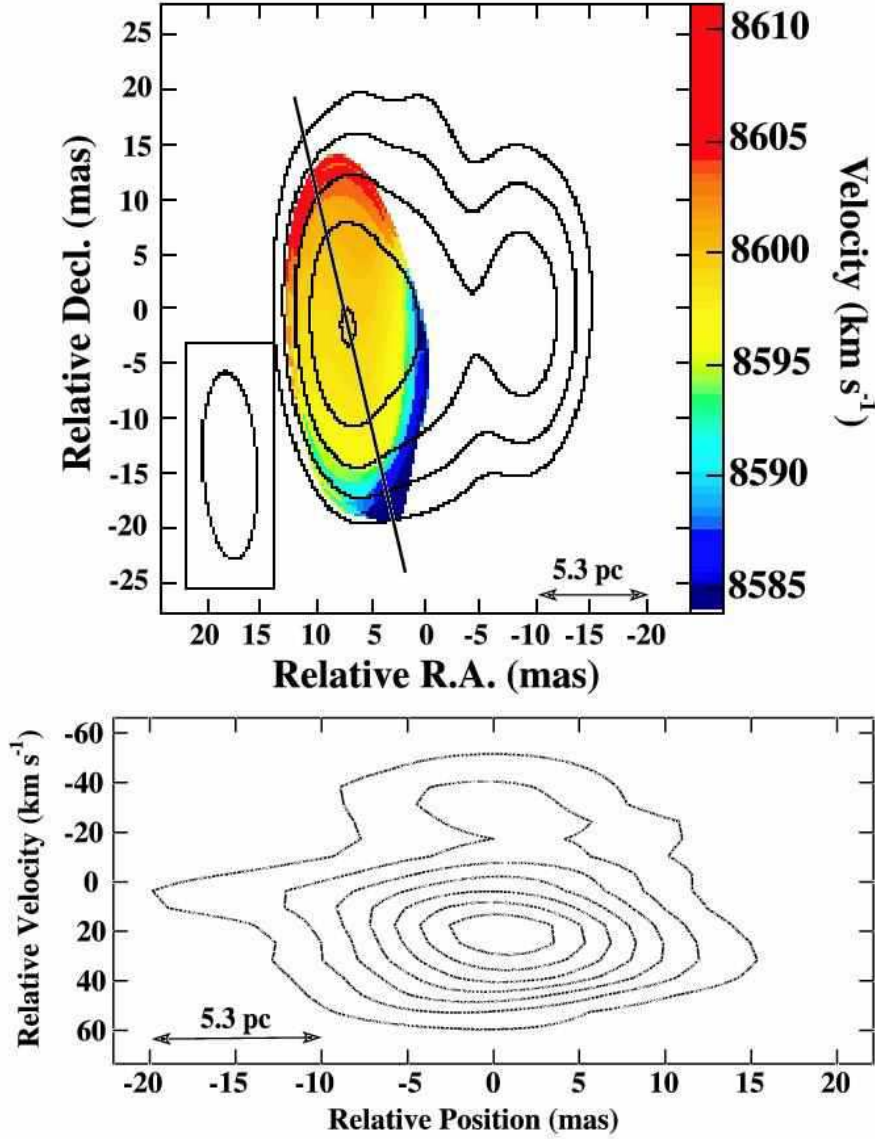


Fig. 6.— *Top*: Velocity field of the strongest H I feature at high spatial resolution, superimposed on the continuum contours with levels at 1, 2, 4, 8, 16 mJy beam $^{-1}$ . The 17  $\times$  5 mas (P.A. 3°) restoring beam is shown in the lower left corner. The point (0,0) is  $\alpha$ (J2000) = 23<sup>h</sup>27<sup>m</sup>56<sup>s</sup>.7097,  $\delta$ (J2000) = 08°46'44".135. *Bottom*: Position-velocity plot of the 21 cm H I absorption along a cut in position angle 14° as shown in the top panel image. The zero point on the velocity scale corresponds to a heliocentric velocity ( $cz$ ) of 8601.1 km s $^{-1}$ . The contour levels of the P-V plot are at (-4, -8, -12, ..., -28)  $\times$  1 $\sigma$  (260  $\mu$ Jy beam $^{-1}$ ).

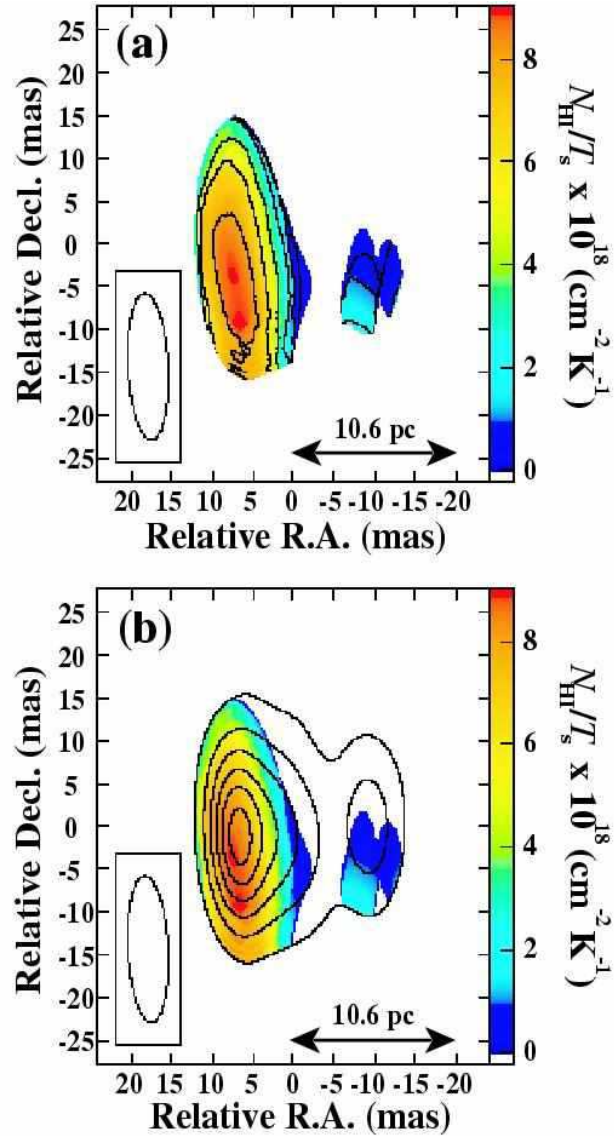


Fig. 7.—  $N_{\text{HI}}/T_s$  images in the velocity range 8626.7–8529.0  $\text{km s}^{-1}$ : (a)  $N_{\text{HI}}/T_s$  color image and contours superimposed; the contours are at  $0.5, 1, 2, 4, 6, 8 \times 10^{18} \text{ cm}^{-2} \text{ K}^{-1}$  (b)  $N_{\text{HI}}/T_s$  color image with continuum contours superimposed; the contour levels are  $2.5, 5, 7.5, \dots, 15 \text{ mJy beam}^{-1}$ . The  $17 \times 5 \text{ mas}$  (P.A.  $3^\circ$ ) restoring beam is shown in the lower left corner of each image. The point  $(0,0)$  is  $\alpha(\text{J2000}) = 23^{\text{h}}27^{\text{m}}56^{\text{s}}.7097$ ,  $\delta(\text{J2000}) = 08^\circ 46' 44''.135$ .

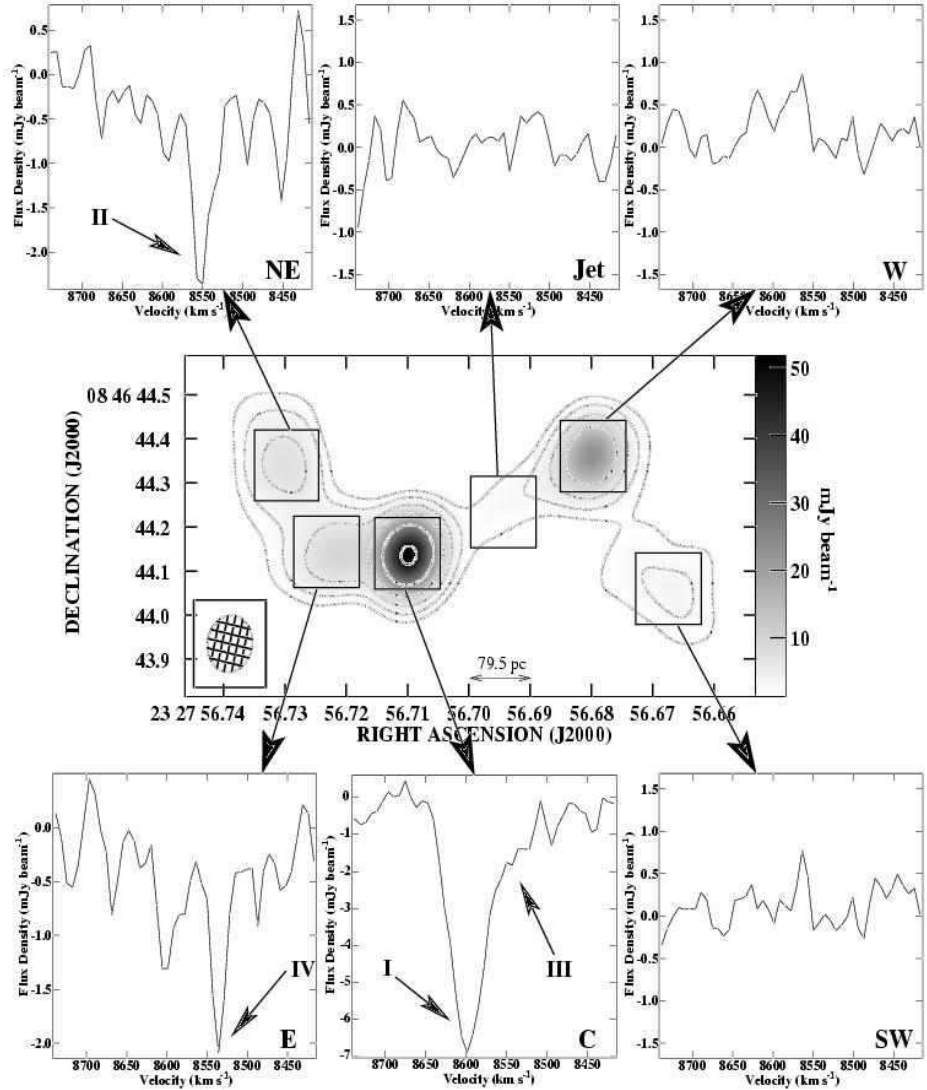


Fig. 8.— H I absorption spectra averaged against the continuum components of NGC 7674 as seen at low spatial resolution at 1380 MHz. The effective velocity resolution of the H I spectra is  $14 \text{ km s}^{-1}$ . The restoring beam size of both the continuum and the H I is  $129 \times 108 \text{ mas}$  in position angle  $-13^\circ$ . The contour levels of the continuum image are at  $-1.5, 1.5, 3, 6, \dots, 48 \text{ mJy beam}^{-1}$ . The rms noise level of the continuum and the H I data are  $85$  and  $570 \mu\text{Jy beam}^{-1}$ , respectively. A two dimensional Gaussian taper falling to 30% at  $1.4 \text{ M}\lambda$  was applied to obtain these images.

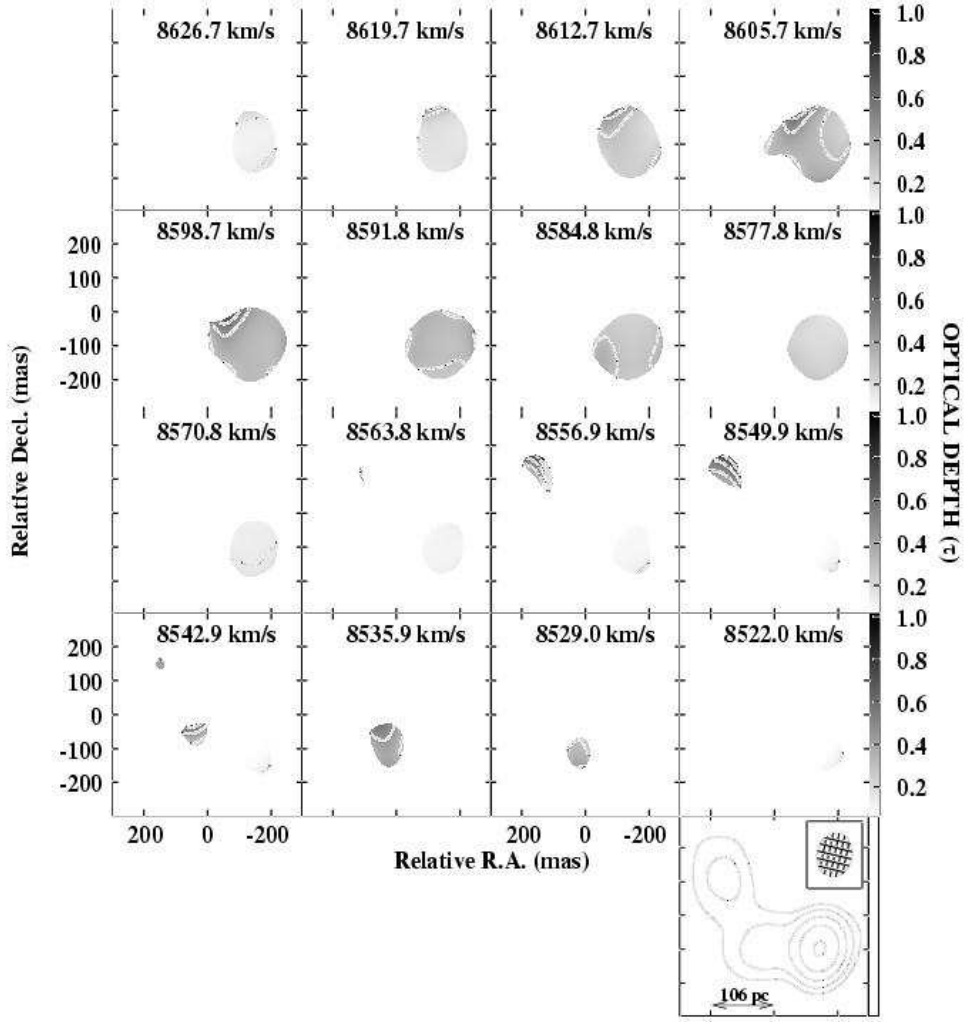


Fig. 9.— Low resolution gray-scale and contour H I optical depth channel images toward the central, eastern, and northeastern components in NGC 7674 in the velocity range 8626.7–8522.0 km s<sup>−1</sup>. The gray-scale range is indicated by the step wedge on the right-side of the images; the contour levels are 0.15, 0.3, 0.45, 0.6, 0.75 and 0.9. At the bottom-right corner a continuum image is shown as a positional reference with levels at 3, 6, 12, 24 and 48 mJy beam<sup>−1</sup>. The restoring beam in these images is 129 × 108 in position angle 13°. The point (0,0) is  $\alpha$ (J2000) = 23<sup>h</sup>27<sup>m</sup>56<sup>s</sup>.7195,  $\delta$ (J2000) = 08°46'44".234.

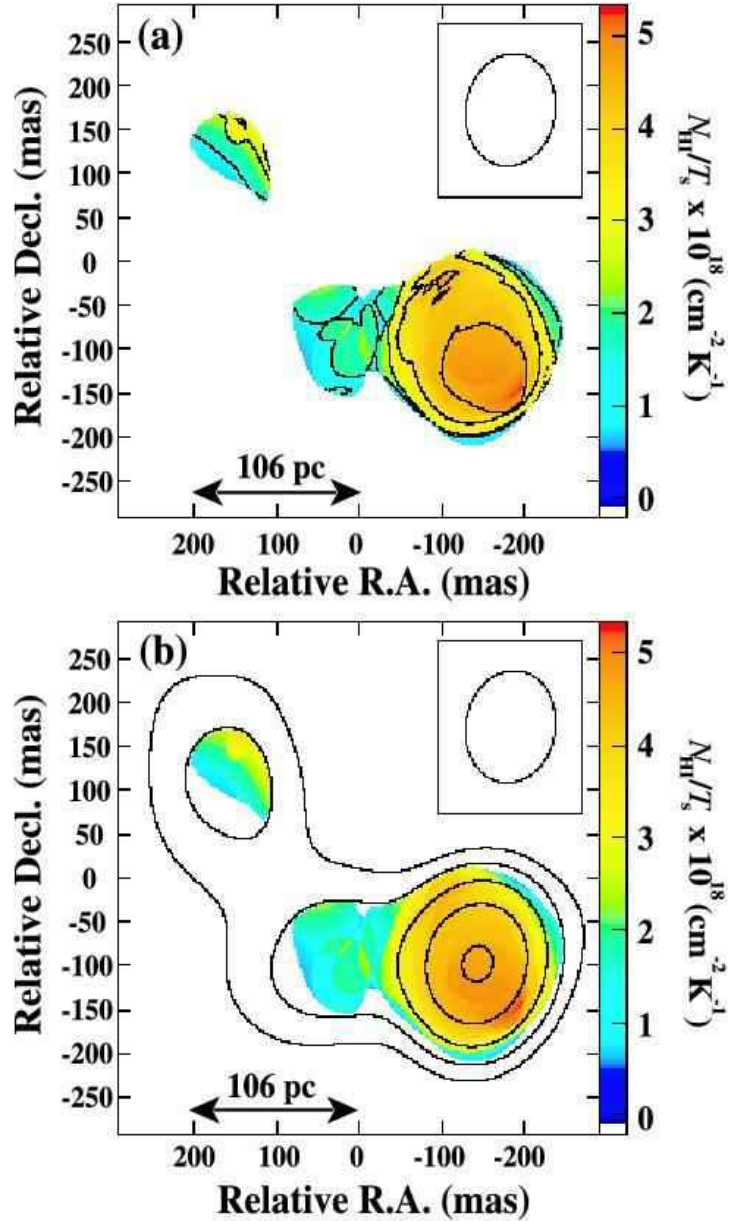


Fig. 10.—  $N_{\text{HI}}/T_s$  images in the velocity range 8626.7–8522.0  $\text{km s}^{-1}$ : (a)  $N_{\text{HI}}/T_s$  color image and contours superimposed; the contours are at  $0.5, 1.5, 2.5, 3.5, 4.5 \times 10^{18} \text{ cm}^{-2} \text{ K}^{-1}$  (b)  $N_{\text{HI}}/T_s$  color image with continuum contours superimposed; the contour levels are  $3, 6, 12, \dots, 48 \text{ mJy beam}^{-1}$ . The  $129 \times 108 \text{ mas}$  (P.A.  $-13^\circ$ ) restoring beam is shown in the upper-right corner of each image. The point  $(0,0)$  is  $\alpha(\text{J2000}) = 23^{\text{h}}27^{\text{m}}56\text{s}.7195$ ,  $\delta(\text{J2000}) = 08^\circ46'44\text{.}234$ .

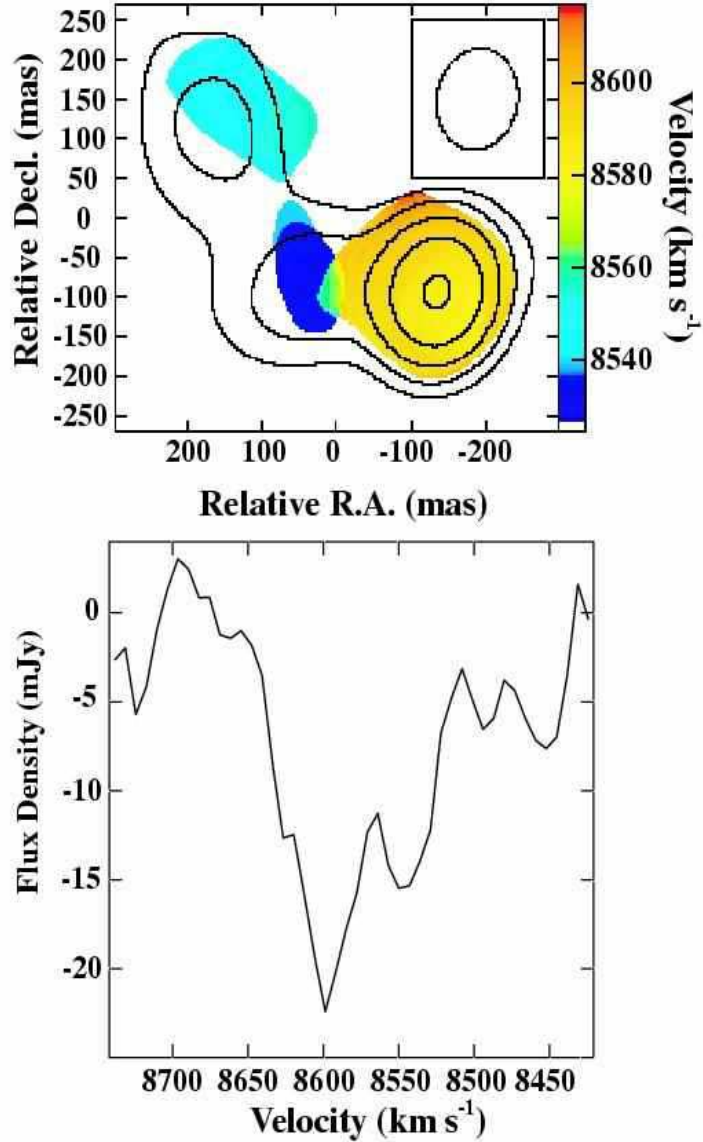


Fig. 11.— *Top*: Velocity field of the H I absorption at low spatial resolution superimposed on the continuum contours with levels at 3, 6, 12, 24, 48 mJy beam<sup>-1</sup>. The 129 × 108 mas (P.A. -13°) restoring beam is shown in the upper-right corner. *Bottom*: Integrated H I 21 cm absorption profile against the whole region where H I absorption is detected at low spatial resolution (129 × 108 mas). The double H I absorption profile is consistent with the two absorption features in the H I spectrum obtained with the 305-m Arecibo radio telescope at 3'3 resolution (Mirabel 1982).

Table 1. PARAMETERS OF THE VLBI OBSERVATIONS OF NGC 7674

Parameters	Values
Observing Date .....	2001 September 15
Observing Array .....	VLBA + Y27 + AR
R.A. (J2000) .....	23 27 56.7097
Dec. (J2000) .....	+08 46 44.135
Total observing time (hr).....	12
Phase-referencing cycle time (min) .....	2.5
Frequency (MHz) .....	1380
Total bandwidth (MHz) .....	16
High resolution ( $11 \times 5$ mas) cont. image rms ( $\mu\text{Jy beam}^{-1}$ ) ..	67
Moderate resolution (20 mas) cont. image rms ( $\mu\text{Jy beam}^{-1}$ ) ..	34
Low resolution ( $92 \times 76$ mas) cont. image rms ( $\mu\text{Jy beam}^{-1}$ ) ..	78
Line velocity resolution ( $\text{km s}^{-1}$ ) .....	14
High resolution ( $17 \times 5$ mas) line image rms ( $\mu\text{Jy beam}^{-1}$ ) ..	260
Low resolution ( $129 \times 108$ mas) line image rms ( $\mu\text{Jy beam}^{-1}$ ) ..	570

Note. — Units of right ascension are hours, minutes, and seconds, and units of declination are degrees, arcminutes, and arcseconds.

Table 2. GAUSSIAN FITS TO THE CENTRAL COMPONENT IN NGC 7674

Source	Relative Position <sup>a</sup> (mas)	Peak (mJy beam <sup>-1</sup> )	Total (mJy)	Major Axis <sup>b</sup> (pc)	Minor Axis <sup>b</sup> (pc)	P.A. <sup>c</sup> ( $^{\circ}$ )	$T_b$ (K)
(1)	(2)	(3)	(4)	(5)	(6)	(7)	(8)
C1 ...	0 , 0	$16.229 \pm 0.006$	$27.060 \pm 0.010$	6.4	4.0	0.16	$21.5 \times 10^7$
C2 ...	7.5W, 0N	$5.023 \pm 0.002$	$11.783 \pm 0.006$	7.8	4.7	5.98	$6.6 \times 10^7$
C3 ...	16.5W, 1N	$5.829 \pm 0.002$	$8.405 \pm 0.003$	6.3	3.5	178.34	$7.3 \times 10^7$

<sup>a</sup>The position (0,0) is  $\alpha$ (J2000) =  $23^{\text{h}}27^{\text{m}}56^{\text{s}}.7101$ ,  $\delta$ (J2000) =  $+08^{\circ}46'44.134$ .

<sup>b</sup>Errors are  $\leq 0.02$  pc

<sup>c</sup>Errors are  $\leq 0.03^{\circ}$

Table 3. GAUSSIAN FITS TO THE WESTERN COMPONENT IN NGC 7674

Source	Relative Position <sup>a</sup> (mas)	Peak (mJy beam <sup>-1</sup> )	Total (mJy)	Major Axis <sup>b</sup> (pc)	Minor Axis <sup>b</sup> (pc)	P.A. <sup>c</sup> ( $^{\circ}$ )	T <sub>b</sub> (K)
(1)	(2)	(3)	(4)	(5)	(6)	(7)	(8)
W1...	0 , 0	$3.229 \pm 0.002$	$12.386 \pm 0.009$	9.7	6.1	174	$4.3 \times 10^7$
W2...	13.5E, 1N	$0.891 \pm 0.001$	$2.231 \pm 0.002$	7.9	4.9	169	$1.2 \times 10^7$
W3...	22.5E, 3N	$1.121 \pm 0.002$	$2.726 \pm 0.004$	8.9	4.2	175	$1.5 \times 10^7$
W4...	34.5E, 6N	$0.628 \pm 0.001$	$2.132 \pm 0.002$	10.0	5.3	164	$0.8 \times 10^7$

<sup>a</sup>The position (0,0) is  $\alpha$ (J2000) =  $23^{\text{h}}27^{\text{m}}56^{\text{s}}6790$ ,  $\delta$ (J2000) =  $+08^{\circ}46'44.369$ .

<sup>b</sup>Errors are  $\leq 0.03$  pc

<sup>c</sup>Errors are  $\leq 0.002^{\circ}$

Table 4. PARAMETERS OF THE CONTINUUM COMPONENTS IN FIGURE 4

Source	Relative Position <sup>a</sup> (mas)	Peak (mJy beam <sup>-1</sup> )	Total (mJy)	Major Axis <sup>b</sup> (pc)	Minor Axis <sup>b</sup> (pc)	P.A. <sup>c</sup> ( $^{\circ}$ )
(1)	(2)	(3)	(4)	(5)	(6)	(7)
C ....	0 , 0	$49.74 \pm 0.01$	$52.74 \pm 0.01$	$49.56 \pm 0.02$	$41.85 \pm 0.02$	17
E.....	168E, 1N	$6.46 \pm 0.02$	$17.64 \pm 0.05$	$77.29 \pm 0.24$	$69.13 \pm 0.32$	78
W....	450W, 226N	$19.71 \pm 0.04$	$25.07 \pm 0.04$	$51.20 \pm 0.10$	$48.60 \pm 0.15$	176
NE...	317E, 213N	$5.59 \pm 0.01$	$20.57 \pm 0.03$	$99.98 \pm 0.18$	$72.01 \pm 0.17$	30
SW ..	633W, 68S	$2.45 \pm 0.01$	$15.73 \pm 0.06$	$144.11 \pm 0.98$	$87.31 \pm 0.65$	164
J.....	-	-	7.9	218	78	116

<sup>a</sup>The position (0,0) is  $\alpha(\text{J2000}) = 23^{\text{h}}27^{\text{m}}56^{\text{s}}.7098$ ,  $\delta(\text{J2000}) = +08^{\circ}46'44''137$ .

<sup>b</sup>Half power width for components with gaussian fits. Linear extent on the plane of the sky for the jet component

<sup>c</sup>Gaussian fit errors are  $\leq 0.002^{\circ}$

Table 5. PROPERTIES OF THE CONTINUUM STRUCTURES

Source	Magnetic Field		Pressure (dyne cm <sup>-2</sup> )
	(1)	(2)	
C ....	$6.3 \times 10^{-4}$		$12.3 \times 10^{-9}$
E.....	$3.0 \times 10^{-4}$		$2.8 \times 10^{-9}$
W....	$3.8 \times 10^{-4}$		$4.5 \times 10^{-9}$
NE...	$2.8 \times 10^{-4}$		$2.5 \times 10^{-9}$
SW ..	$1.6 \times 10^{-4}$		$0.8 \times 10^{-9}$

Table 6. GAUSSIAN FITS PARAMETERS OF THE H I ABSORPTION FEATURES AT HIGH RESOLUTION

Feature	Velocity (km s <sup>-1</sup> )	$\Delta v_{\text{FWHM}}$ (km s <sup>-1</sup> )	$\tau_{\text{peak}}$	$N_{\text{HI}}/T_{\text{s}}$ (cm <sup>-2</sup> K <sup>-1</sup> )	$N_{\text{HI}}$ (cm <sup>-2</sup> )
(1)	(2)	(3)	(4)	(5)	(6)
1 .....	$8603.1 \pm 0.7$	$35.4 \pm 2.3$	$0.412 \pm 0.025$	$(2.8 \pm 0.3) \times 10^{19}$	$(2.8 \pm 0.3) \times 10^{21}$
2 .....	$8577.6 \pm 4.8$	$98.3 \pm 7.1$	$0.164 \pm 0.028$	$(3.1 \pm 0.6) \times 10^{19}$	$(3.1 \pm 0.6) \times 10^{21}$
3 .....	$8573.3 \pm 1.8$	$22.5 \pm 4.3$	$0.298 \pm 0.051$	$(1.3 \pm 0.4) \times 10^{19}$	$(1.3 \pm 0.4) \times 10^{21}$
4 .....	$8534.3 \pm 1.2$	$18.0 \pm 2.9$	$0.337 \pm 0.047$	$(1.2 \pm 0.3) \times 10^{19}$	$(1.2 \pm 0.3) \times 10^{21}$

Table 7. GAUSSIAN FIT PARAMETERS OF THE H I ABSORPTION FEATURES AT LOW RESOLUTION

Feature	Velocity (km s <sup>-1</sup> )	$\Delta v_{\text{FWHM}}$ (km s <sup>-1</sup> )	$\tau_{\text{peak}}$	$N_{\text{HI}}/T_{\text{s}}$ (cm <sup>-2</sup> K <sup>-1</sup> )	$N_{\text{HI}}$ (cm <sup>-2</sup> )
(1)	(2)	(3)	(4)	(5)	(6)
I .....	$8600.3 \pm 1.1$	$49.8 \pm 2.5$	$0.369 \pm 0.016$	$(3.5 \pm 0.2) \times 10^{19}$	$(3.5 \pm 0.3) \times 10^{21}$
II .....	$8550.7 \pm 1.8$	$30.8 \pm 4.4$	$0.647 \pm 0.080$	$(3.8 \pm 0.7) \times 10^{19}$	$(3.8 \pm 0.6) \times 10^{21}$
III .....	$8544.0 \pm 8.9$	$165.0 \pm 14.6$	$0.104 \pm 0.010$	$(3.3 \pm 0.3) \times 10^{19}$	$(3.3 \pm 0.3) \times 10^{21}$
IV .....	$8536.3 \pm 1.7$	$22.6 \pm 4.0$	$0.434 \pm 0.067$	$(1.9 \pm 0.4) \times 10^{19}$	$(1.9 \pm 0.4) \times 10^{21}$